# Quality and matching performance analysis of three-dimensional unraveled fingerprints

**Yongchang Wang**
University of Kentucky
1 Quality St Ste 800, Lexington, KY, 40507

**Qi Hao**
University of Alabama
210 Houser Hall, Tuscaloosa, AL, 35487

**Abhishika Fatehpuria**
**Laurence G. Hassebrook**
**Daniel L. Lau**
University of Kentucky
1 Quality St Ste 800, Lexington, KY, 40507
E-mail: lgh@engr.uky.edu, dllau@engr.uky.edu

**Abstract.** The use of fingerprints as a biometric is both the oldest mode of computer aided personal identification and the most relied-upon technology in use today. However, current acquisition methods have some challenging and peculiar difficulties. For higher performance fingerprint data acquisition and verification, a novel non-contact 3D fingerprint scanner was investigated, where both the detailed 3D and albedo information of the finger is obtained. The obtained high resolution 3D prints are further converted into 3D unraveled ones, to be compatible with traditional 2D automatic fingerprint identification systems. As a result, many limitations imposed upon conventional fingerprint capture and processing can be reduced by the unobtrusiveness of this approach and the extra depth information acquired. In order to compare the quality and matching performances of 3D unraveled with traditional 2D plain fingerprints, in this paper, both 3D prints and their 2D plain counterparts were collected. The print quality and matching performances are evaluated and analyzed by using National Institute of Standard Technology fingerprint software. Experimental results show that the 3D unraveled print outperforms the 2D one in both quality and matching performances. © *2010 Society of Photo-Optical Instrumentation Engineers* *DOI: 10.0000/000.000*

Subject terms:

Paper 000000R compiled July 26, 2010.

## 1 Introduction

Biometrics is an automated method of identifying a person based on a physiological or behavioral characteristic. Among all the bio-identification systems, fingerprint based systems have gained immense popularity[1–5] due to the high level of uniqueness attributed to fingerprints and favorable technical factors like compact and inexpensive sensors and fast computing software. Automatic Fingerprint Identification Systems (AFIS), developed initially for use by law enforcement agencies, are being widely used for general identification and fraud prevention. Higher matching performance can be achieved if a fingerprint's quality is sufficiently good and the overall database integrity is improved.[6]

Traditional fingerprint acquisition is performed in 2D using contact methods which have evolved over the last century, from ink (rolled or plain) to capacitive, ultrasonic, pyroelectric, thermal, and optoelectronic approaches.[7–10] In many applications that require high precision fingerprints, limitations are imposed upon the current fingerprint capture technologies[11–13] including:

1) obligatory maintenance of a clean sensor or prism surface;

2) uncontrollability and non-uniformity of the finger pressure on the device;

3) permanent or semi-permanent change of the finger ridge structure due to injuries or heavy manual labors;

4) residues from the previous fingerprint capture;

5) data distortion under different illumination, environmental, and finger skin conditions; and

6) extra scanning time and motion artifacts incurred in technologies that require finger rolling.

The majority of these limitations arise due to the physical contact of the finger surface with the sensor plate or the nonlinear distortion introduced by the 3D-to-2D mapping during image acquisition.[14] To address these issues, several novel technologies have been developed[15–18] that avoid direct contact between the sensor and the skin.

Parziale *et al*[17] proposed a multi-camera, touchless, fingerprint scanner that acquires different finger views combined together to provide a 3D representation of the fingerprint. Due to the lack of contact between the elastic skin of the finger and any rigid surface, the acquired images preserve the fingerprints "ground-truth" without skin deformation during acquisition. However employing the shape-from-silhouette scanning technique, the ridge information is obtained from the surface reflection variation (i.e. albedo) information. Thus, the fingerprint is sensitive to surface color, surface reflectance, geometric factors, and some other effects. And since the accurate 3D information is not available when unraveling their 3D print into a 2D print compatible with current 2D AFIS,[19] the distortion caused by unraveling is hard to control.

In order to achieve significant improvements over the manner in which fingerprint images are currently acquired, a non-contact 3D fingerprint scanner was investigated employing structured light illumination (SLI) as a means of extracting the 3D shape of fingerprint ridges using multiple, commodity digital cameras in conjunction with a novel SLI technique to acquire the fingerprint scan without physical contact between sensor and finger. The non-contact 3D fingerprint scanner was developed by Flashscan3D LLC. and the University of Kentucky. As shown in Fig. 1, the system mainly

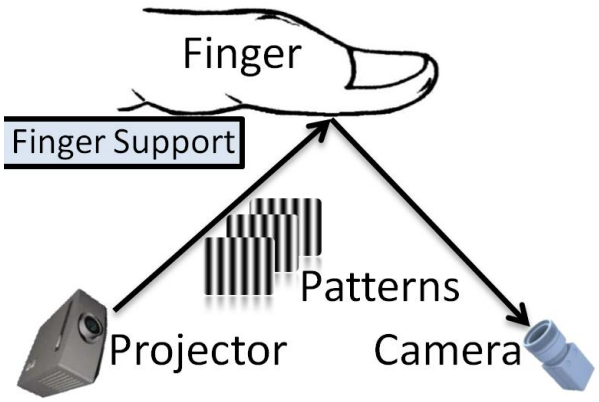


**Fig. 1** The non-contact 3D fingerprint scanner.

consists of a projector and a camera. To minimize the effects of finger movement during scanning and depth of focus, the fingernail rests against a support. The system relies on 3D image acquisition through an SLI approach where the phase measuring profilometry (PMP) pattern strategy[20–22] is employed. The advantages of the non-contact 3D fingerprint scanning and processing technology include:

1) non-contact defuses distortion that exists in conventional fingerprint acquisition system;
2) simultaneous acquisition of both albedo and ridge depth information of fingers;
3) automated fingerprint entry in no need of interaction with the operator;
4) real-time feedback for users to make position adjustment;
5) robustness to contamination of fingers and residues of previous users;
6) robustness to clutter and fraud because of the difficulties in faking 3D fingerprints;
7) fast scanning (0.7 second) and data processing (less than 1 second); and
8) low cost by using an off-the-shelf commodity camera and projector.

Furthermore to be compatible with 2D AFIS, we developed a fit-tube algorithm which unravels the 3D print into 2D. Because both texture and ridge depth information are available in the 3D scans, ridge information can be extracted from both albedo and depth for improved ridge detail.

In this paper, we present a thorough evaluation of the resulting unwrapped fingerprint scans produced by the 3D scanner, which we compare to scans produced by a traditional 2D scanner, the Cogent CSD450. For this purpose, we employ the National Institute of Standard Technology (NIST) quality algorithms where experimental results show that the measured quality metrics of the 3D prints follow similar patterns of traditional 2D prints. Thus, we demonstrate that the statistical metrics, generated by the NIST algorithm, for traditional 2D fingerprint quality evaluation, can also be used to evaluate the quality of unraveled 3D prints. And comparisons between the quality metrics of 2D and 3D prints indicate that the 3D prints achieve higher overall image quality, higher local image quality, more high quality minutiae, and higher classification confidence number than scans recorded by the contact-based scanner. Finally, we employ the NIST matching algorithm, which is based on minutiae matching between prints,where experimental results show that the 3D prints achieve better matching performance than those collected on the 2D scanner.

The rest of this paper is organized as follows. Sec. 2 describes the 3D acquisition setup. Sec. 3 presents the methods to convert 3D scans to 2D flat equivalent finger images. Sec. 4 discusses and compares the fingerprint quality evaluations of unraveled 3D and 2D prints. Sec. 5 presents and compares the matching performances of unraveled 3D and 2D prints. Sec. 6 outlines the conclusion and future works.

## 2 Fingerprint Acquisition

The 3D fingerprint scanner employs the PMP technique for 3D data acquisition. Compared to other structure light algorithms like single spot, light stripe, and gray code projection, the PMP technique obtains the same precision using fewer patterns[23] where the projected light pattern is expressed as

$$I_n^p(x^p, y^p) = A^p + B^p \cos(2\pi f \frac{y^p}{L} + 2\pi n/N), \quad (1)$$

where $(x^p, y^p)$ are the projector coordinates, $A^p$ and $B^p$ are projector constants, the subscript $n$ represents the pattern index, $N$ is the total number of patterns, $f$ is the frequency of the sine wave, and $L$ is the length of the sine wave (length or height resolution of the projector).[24]

From the camera viewpoint, the captured image is distorted by the object topology in terms of

$$I_n^c(x^c, y^c) = A^c(x^c, y^c) + B^c(x^c, y^c) \cos[\phi(x^c, y^c) - \frac{2\pi n}{N}], \quad (2)$$

where $I_n^c(x^c, y^c)$ represents the intensity of $n^{th}$ pattern at pixel location $(x^c, y^c)$ of the captured image, $A^c$ and $B^c$ are the albedo and modulation information, and $\phi(x^c, y^c)$ represents the phase value at pixel location $(x^c, y^c)$ of the captured sine wave pattern. Thus, $\phi(x^c, y^c)$ can be computed from the captured images as follows

$$\phi(x^c, y^c) = \arctan\left[\frac{\sum_{n=1}^{N} I_n^c(x^c, y^c)\sin(2\pi n/N)}{\sum_{n=1}^{N} I_n^c(x^c, y^c)\cos(2\pi n/N)}\right]. \quad (3)$$

As the phase value can only be estimated between $[-\pi, \pi]$, the value of projector coordinate is between $[-1/2f, 1/2f]$, which will limit the measurable depth range of objects.

Once the value of $\phi(x^c, y^c)$ is obtained, the projector coordinate $y^p$ of a 3D point with a camera coordinate $(x^c, y^c)$ can be recovered from

$$y^p(x^c, y^c) = \phi(x^c, y^c)\frac{L}{2\pi f}. \quad (4)$$

Based on $(x^c, y^c, y^p(x^c, y^c))$, the 3D depth can be computed using the perspective projection matrix obtained through a

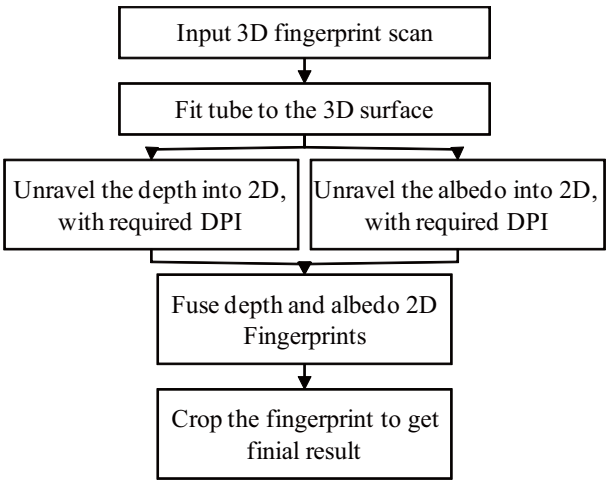


**Fig. 3** Flowchart for the 3D data processing.

joint projector and camera calibration.[25,26] Further, the albedo image is:

$$A^c(x^c, y^c) = \frac{1}{N}\sum_{n=1}^{N} I_n^c(x^c, y^c), \tag{5}$$

In the scanner, a total of $N = 10$ phase shift patterns with frequency $f = 16$ cycles/field of view is chosen to make a trade-off between scanning time and resolution. The system takes 0.7 second for scanning with the obtained image resolution is as high as $1,420 \times 2,064$. Figure 2 shows the a 3D fingerprint obtained by the scanner, where the detailed albedo and 3D information are obtained.

## 3 Virtual Flattening

In order to unravel the 3D prints into 2D, we developed the fit-tube algorithm from the fit-sphere algorithm.[18] This section summarizes the fit-tube algorithm. The 3D fingerprint is composed of point clouds where each point, within the cloud, corresponds to a pixel of the camera and is assigned a position in 3-D space along with a gray-scale albedo value (Fig. 2). Traditional 2-D fingerprint scans are extracted from these clouds through a virtual unraveling process summarized by the flowchart of Fig. 3. To start, the unraveling algorithm fits a deformable tube to the 3-D point cloud, achieved by deriving best fitting circles, spaced 0.508 mm (500 rings per inch) apart, along the vertical axis of the finger. Along each ring, two 1-D, discrete-time, signals are extracted at a sampling period of 0.508 mm (500 samples per inch). The first signal is the distance between the ring of fixed radius and the nearest neighboring point within the cloud, while the second is the albedo signal for these same points.

The signal representing the distance between scan points and the best-fit ring is further processed by means of band-pass filtering, where the high-frequency band contains mostly process noise from the camera and projector while the low-frequency band represents the difference in shape of the finger versus the best-fit tube. The preserved mid-frequency band contains fingerprint ridge and valley information that are rescaled, in value, to range from 0 to 255 (8-bits per pixel grayscale). Now by lining up the 1-D signals, side-by-side, for all rings forming the deformable tube, two separate, flattened fingerprint images are created, where the first image is the albedo fingerprint corresponding to $A^c(x^c, y^c)$, in Eq. 5, while the second is the 3-D print obtained from $(x^c, y^c, y^p(x^c, y^c))$. It is this second signal that is unique to the SLI scanning method; whereas, the albedo component is consistent with that produced by Parziale *et al*.[17]

In order to take advantage of this added information provided by depth, the two scans need to be fused together by first converting the two images to a common reference space by means of binarizing the grayscale unraveled prints. Then, NIST MINDTCT algorithm (see in Sec. 4) is employed to measure the local quality of the two images. The MINDTCT divides the images into 8×8 pixel blocks and then assigns an image quality score to each block. A composite image is then produced by choosing, on a block by block basis, the image with the better local image quality. In this way, the composite image will always have a higher average local image quality score than either of the two component images. As a final step, out of focus regions of the fingerprint, along the outer ring of the observed scan area, are cropped out of the scan since these regions have poor PMP signal strength and, hence, poor ridge detail. But even with this cropping, our experiments show a scan area approximately $4.4\%$ larger than that of the Cogent CSD450 for the same subject set. Examples of unraveled 3D and traditional 2D fingerprints and their quality maps are shown in Fig. 4, where darker color represents lower quality and the black area is the background with no information. The poor quality area in the center of the prints is due to the high curvature of the ridges.[27]

## 4 Image Quality Analysis

Many biometric studies have addressed the problem of assessing fingerprint image quality[28–30] looking at features like local orientation information, global uniformity and continuity, amplitude and variance of spectral bases, or effective feature number of fingerprint images. Studies have also been performed showing that image quality assessment can accurately predict matching performance[31] where scanners with higher average image quality scores achieve higher recognition performance.[27]

For measuring the scan quality of 3D fingerprint scans, we rely on the NIST Biometric Image Software (NBIS) quality and matching performance analysis tools. The NBIS is public domain software organized into several major systems.[27] First, the PCASYS system is a prototype classifier that separates fingerprints into basic pattern-level classes such as *arch, left loop, right loop, scar, tented arch,* or *whorl*. PCASYS also outputs an estimated posterior probability of the hypothesized class, which is a measure of the confidence that may be assigned to the classifier's decision. Improved scan quality will result in higher PCASYS confidence levels, closer to 1, in its corresponding class.

The MINDTCT system takes a fingerprint image and locates all minutiae in the image, assigning to each minutia point its location, orientation, type, and quality. To locally analyze the image, MINDTCT divides the image into a grid of blocks with 8×8 pixels in each block and assesses the quality of each block. The information in these maps is in-

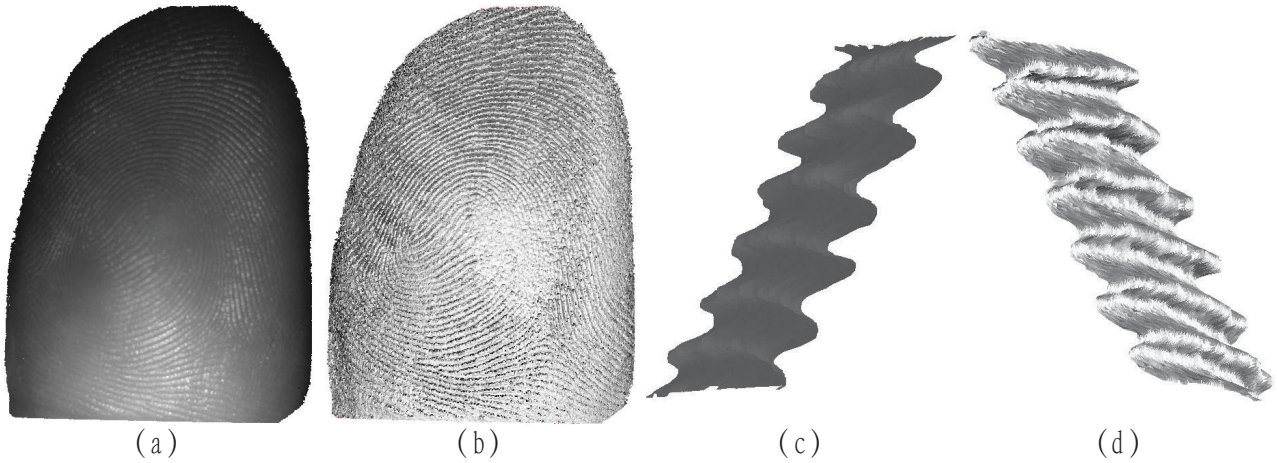


**Fig. 2** A 3D fingerprint illustrated in (a) and (c) albedo (surface reflectance variations) and (b) and (d) in 3D where (c) and (d) show a cropped portion of the fingerprint.

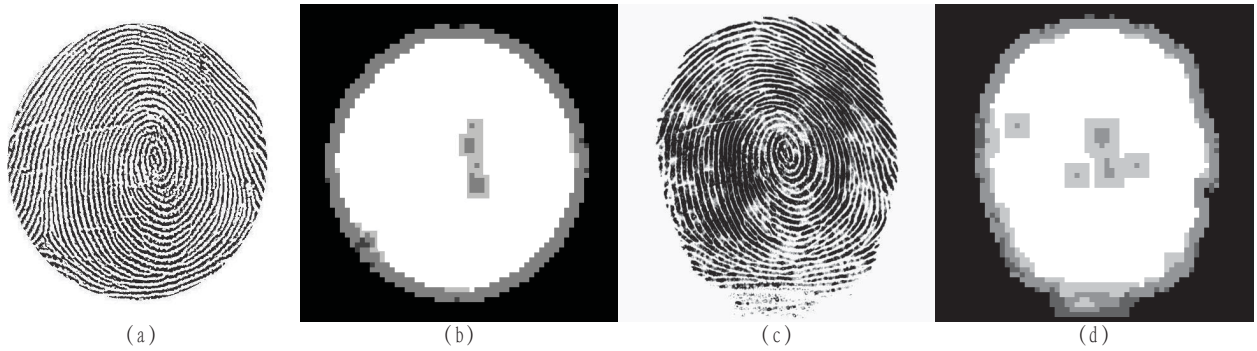


**Fig. 4** (a) A 3D unraveled fingerprint. (b) Quality map of the 3D unraveled fingerprint. (c) A traditional 2D fingerprint. (d) Quality map of the traditional 2D fingerprint.

tegrated into one general map and contains 5 levels of quality (4 being the highest quality and 0 being the lowest). MINDTCT also computes quality or reliability measures to be associated with each detected minutiae point. A quality value in the range from 0.01 to 0.99 is assigned to each minutiae, where a quality number greater than 0.75 are considered to be highly reliable.[27] The better the image quality, the higher the number of reliable minutiae detected.

The NFIQ system measures the overall quality of a fingerprint image sample. NFIQ classifies the fingerprint images into 5 classes wherein a quality number 1 represents excellent quality and 5 poor quality. Several example fingerprint images along with the corresponding image quality metrics are shown in Fig. 5 where we note that a superior scanning technology should generate a higher number of reliable minutiae (greater than 20), more blocks with high local quality (zone4 representing the highest local quality), and a lower overall image quality number (1 representing the highest overall quality).

Now having the above set of image quality metrics, our goal is to analyze and compare the performance of the non-contact, SLI scanner versus a commercially available system (the Cogent CSD450) using a common subject pool. For this purpose, we constructed a fingerprint composed of 440 3D as well as 440 conventional fingerprint scans taken from 12 human subjects. For the 3D prints, all ten fingers of each subject were scanned using the SLI prototype scanner, described in Sec. 2, that were unraveled into 2D equivalent images, as described in Sec. 3, and processed with the NIST filters, described above. The corresponding 2D plain images were similarly processed by the NIST filters. Statistical analysis of the NBIS metrics was performed using the Sigma Stat software (SPSS Inc. , IL) and the data was evaluated with one-way ANOVA. All pairwise, multiple comparisons were conducted with the Turkey method[32] where statistical significance was considered when the $p$ value is less than 0.05.

### 4.1 *2D Fingerprint Analysis*

Looking first at the scan quality metrics applied to traditional 2D fingerprint scans, Fig. 6 (a) illustrates the distributions of local image quality scores versus overall image quality. From these distributions, it can be seen that:

- as the overall quality of the fingerprints decreases from 1 (best) to 5 (unusable), the number of $8 \times 8$ pixel blocks with the best local image quality score (zone4) also decreases; whereas, the number of blocks in zones 1-3 increases;
- the number of $8 \times 8$ pixel blocks with the best local quality, zone4, among different overall image qual-

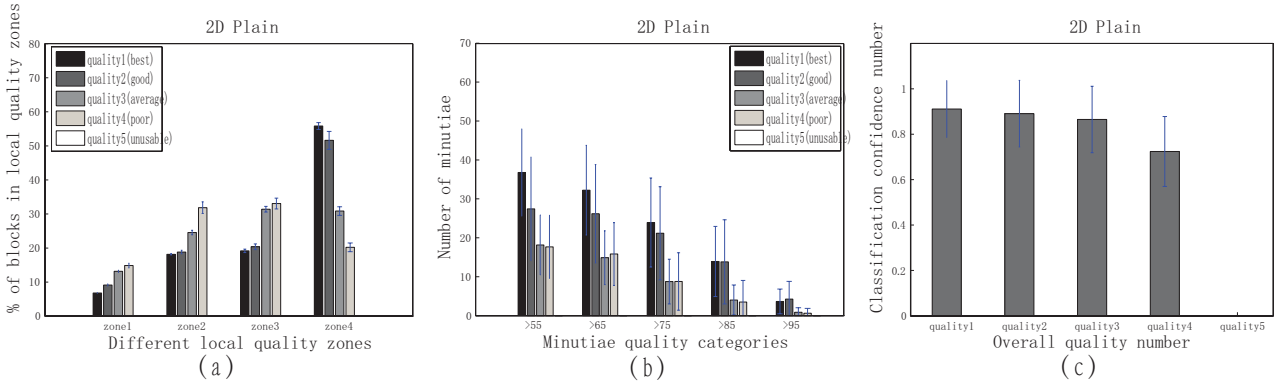


**Fig. 6** Quality analysis for 2D plain fingerprint images. (a) Distributions of informative blocks over local quality zones with respect to overall quality numbers. (b) Distributions of minutiae over minutiae quality numbers with respect to overall image quality numbers. (c) Plot of classification confidence numbers with respect to overall quality numbers.

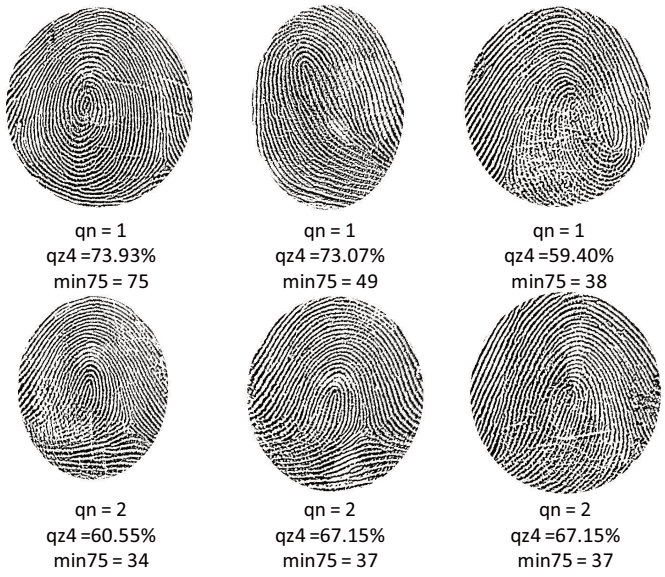


**Fig. 5** Six unraveled 3D fingerprints with their corresponding quality metrics. The qn is the overall quality number with 1 as the highest overall quality. The qz4 represents the percentage of highest local quality blocks. And min75 is the number of reliable minutiae.

ities (1∼5) are significantly different (with $p$ values less than 0.001); and

- the number of $8\times8$ pixel blocks with lesser local quality lack consistent statistical properties among different overall image qualities and cannot be used to evaluate scanner performance.

These observations are summarized by saying that, with regards to local image quality, only the number of $8 \times 8$ pixel blocks in the best local quality zone (zone4) is useful for evaluating 2D plain fingerprints.

With regards to minutiae quality scores, Fig. 6 (b) shows the distributions of the number of detected minutiae versus their minutiae quality scores, greater than 0.55, 0.65, 0.75, 0.85 and 0.95, versus overall image quality. It can be observed from these distributions that the number of minutiae in categories >85 and >95, do not decrease in a statistically significant way with the overall quality number; hence, minutiae quality numbers greater than either 0.85 or 0.95 are not reliable measures for quantifying scanner performance. On the other hand, reliable minutiae in categories of >55, >65, and >75 follow similar patterns, decreasing as the overall quality decreases. Statistical analysis shows a significant difference for all pairwise comparisons in these three categories with $p$ values less than 0.01. Moreover, Tabassi *et al*[27] observed that, generally, fingerprints having 20 minutiae with reliability greater than 0.75 are more likely to be identified correctly by fingerprint matching systems. Thus, the number of minutiae with reliability greater than 0.75 will be our sole metric for evaluating scan quality using minutiae quality scores.

As a final measure of scan quality using 2D fingerprint scans, Fig. 6 (c) shows the classification confidence numbers, obtained by PCASYS, with respect to overall image quality. These confidence scores shows no statistically significant difference for the best, good, and average quality fingerprints, but it reduces significantly as the overall quality of fingerprints further deteriorates. So the classification confidence number, especially for the comparison between images above and below average quality, can be a fourth metric for 2D plain fingerprints evaluation.

### 4.2 *3D Fingerprint Analysis*

Looking now at fingerprint scans acquired through SLI, Fig. 7 (a) illustrates the distributions of local image quality scores versus overall image quality where it can be seen that the 3D print case is similar to that of the 2D print. However, there is difference: as the overall quality of the fingerprints decreases from 1 (best) to 5 (unusable), the number of $8 \times 8$ pixel blocks in the highest of the four local image quality scores, zone4, also decreases, which not as convincingly as for 2D prints. These observations are summarized by saying that only the number of $8 \times 8$ pixel blocks with local quality score 2 and 4 are useful for evaluating 3D fingerprints.

With regards to minutiae quality scores of unraveled 3D prints, Fig. 7 (b) shows the distributions of the number of detected minutiae. It can be seen that for unraveled 3D prints the numbers of minutiae in all categories have a similar pattern: roughly decreasing as the overall image quality de-

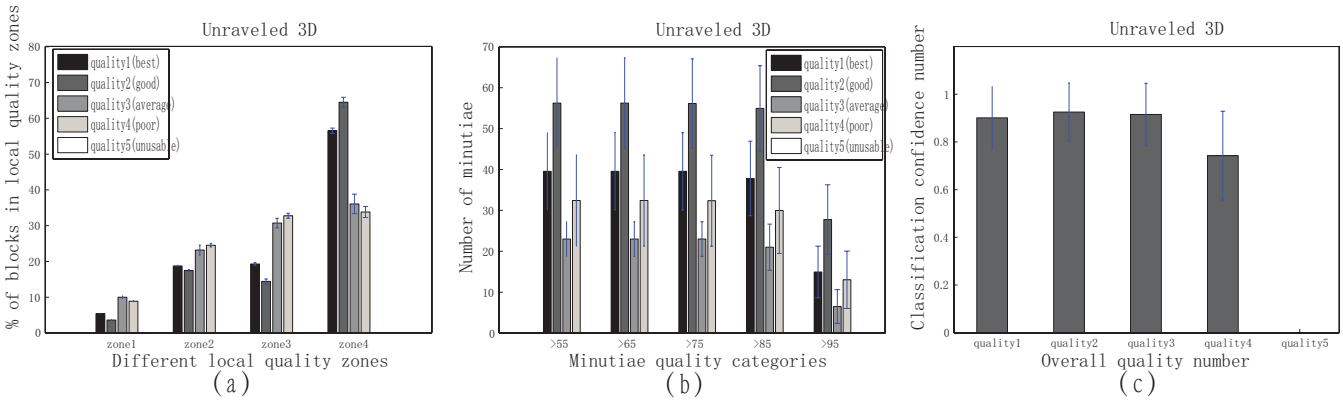


**Fig. 7** Quality analysis for unraveled 3D fingerprints. (a) Distributions of informative blocks over local quality zones with respect to overall quality numbers. (b) Distributions of minutiae over minutiae quality numbers with respect to overall image quality numbers. (c) Plot of classification confidence numbers with respect to overall image quality numbers.

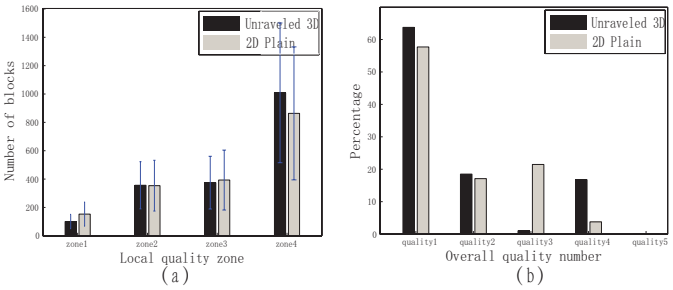


**Fig. 8** (a) The distributions of informative blocks over different local quality zones for 2D plain fingerprints and unraveled 3D fingerprints. (b) Distributions of samples over different overall image quality numbers.

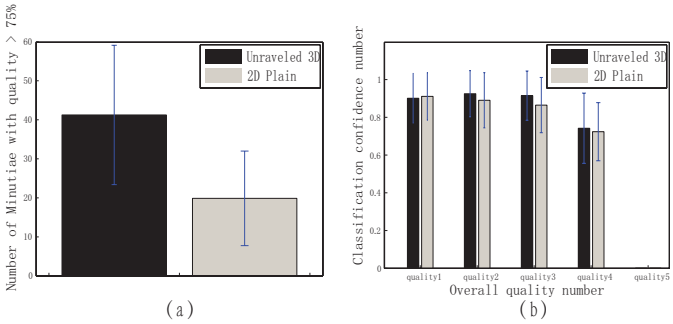


**Fig. 9** (a) Number of high quality minutiae for 2D plain fingerprints and 3D unraveled fingerprints. (b) Classification confidence numbers with respect to different image quality numbers.

creases from best and good to average and poor. The number of minutiae with reliability greater than 0.75 shows a pattern similar to that observed for 2D fingerprints: significantly higher for high overall quality (best and good) images than for low overall quality (average and poor) images. Similar as in the 2D case, we also chose the number of minutiae with reliability greater than 0.75 for evaluating unraveled 3D print quality using minutiae quality scores.

Figure 7 (c) shows the classification confidence numbers with respect to overall image quality numbers for unraveled 3D prints. Similar as the 2D case, the confidence number shows no statistically significant difference, but it reduces significantly for images with the poor overall quality. Thus, as in 2D plain, the contrast between the fingerprints above and below the average quality becomes useful for the quality evaluation of unraveled 3D fingerprints.

The above results show that all the statistical metrics, generated by the NIST software, for traditional 2D fingerprint quality evaluation, can also be used to evaluate the quality of unraveled fingerprints obtained from the unraveled 3D scans. The scanner performance can be quantified by the scanned image quality.

### 4.3 *Comparing 2D and 3D*

For a quantitative analysis of 2D versus 3D fingerprint scanners, we compared the 2D plain fingerprints with the unraveled 3D fingerprint images using the following indexes: 1) the distributions of informative blocks over different local qualities (zones); 2) the distributions of fingerprint over different overall quality numbers; 3) number of high quality minutiae with reliability greater than 0.75; and 4) confidence number with respect to different overall quality numbers. As shown in Fig. 8 (a), the 3D unraveled fingerprints achieve more blocks in local quality zone 4 (best) than the traditional 2D prints.

Figure 8 (b) shows the distributions of image qualities for 2D and 3D data sets where 3D prints have a higher percentage of highest-quality images (63.75%) whereas 57.71% of 2D fingerprints score this same quality rating. But given the fact that the Cogent CSD450 rejects scans of extremely poor quality, the percentage of highest quality scans acquired by the CSD450 is artificially high. So for a fair comparison in average overall quality numbers, we can reject an equal number of poorest quality scans from those collected by the 3D scanner. By doing so, the average overall image quality of 3D prints is 1.1519, whereas for 2D prints, the average image quality score is 1.7125.

Figure 9 (a) shows the comparison between the average minutiae number with quality greater than 0.75 for 3D and 2D prints. The 2D samples have 19.88 qualified minutiae on average, while the 3D samples have 41.25. More specifically in terms of qualified minutiae number, the 2D fingerprints

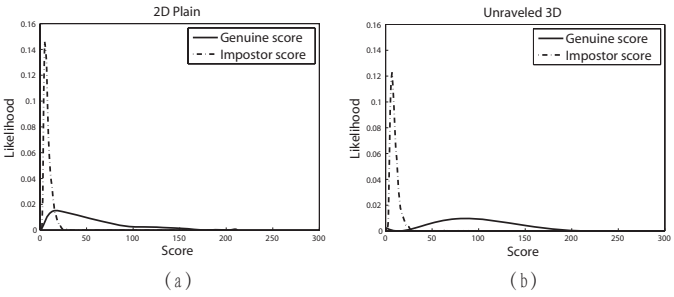


**Fig. 10** Distributions of genuine and impostor scores for (a) 2D plain fingerprints and (b)unraveled 3D fingerprints.

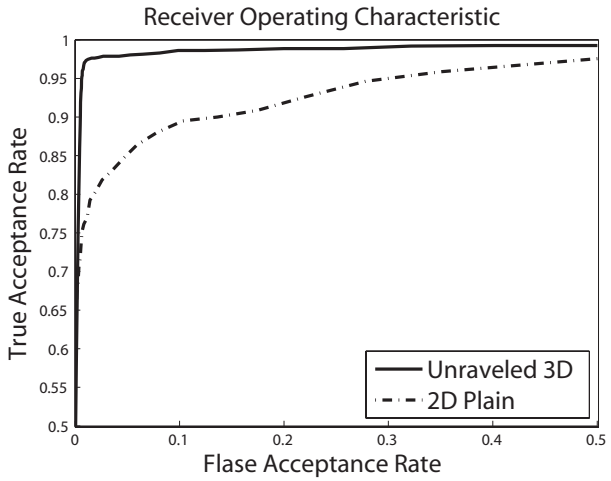


**Fig. 11** Receiver Operating Characteristics (ROCs) of 2D plain and unraveled 3D fingerprints.

score 23.92, 21.16, 8.75, and 8.78 for overall quality number from 1 to 4; the 3D fingerprints score 39.54, 56.14, 23.00, and 32.37, respectively.

In the previous sections, the confidence number showed no statistically significant difference for image quality numbers of 1 to 3, but it dropped significantly for images with quality number 4. From Fig. 9 (b), it can be seen that the 3D unraveled prints achieve a higher average confidence number in both high (qn$\leq$ 3) and low (qn$>$ 3) overall quality prints. Given the fact that the quality of center scan area of a fingerprint is what the NIST classification software is most concerned with, Fig. 9 (b) also suggests that, as the overall image quality decreases, the center area quality of the 3D fingerprint does not drop as significantly as it does for 2D prints.

## 5 Matching Performance

The BOZORTH system is NBIS' tool for matching two sets of minutiae in a rotationally independent manner. The algorithm transforms each set of minutiae into a specialized rotationally invariant graph. To compute a matching score between two fingerprints, the algorithm iteratively searches between both fingers' graphs for subsets that are "compatible", i.e. co-ordinate locations and orientations of the minutiae represented, within the subgraphs, are similar enough to each other based on the defined tolerances. The more nodes contained within a compatible subgraph, the higher the accumulated match similarity score.

Here, the similarity scores of a genuine (i.e. among the same person) comparisons are called genuine scores, while the similarity scores of imposter (i.e. among different persons) comparisons are named imposter scores. Since for different fingers, e.g. thumb and index finger, the basic shape is different, the imposter scores are generally low. To perform reasonable and efficient analysis of the 3D system, we only matched the same finger from different persons, where for the same finger there are two randomly selected scans to get one imposter score. For each data set, there are 1,228 genuine scores, and 11,627 imposter scores. The higher similarity score, the higher the likelihood that these fingerprints come from the same finger. Figure 10 shows the histogram of genuine and imposter scores for all the subjects in both traditional 2D and unraveled 3D databases.

Using the BOSORTH3 algorithm, the better fingerprint scanner system should yield a clearer distinction between genuine and imposter score distributions. Overlapping of genuine and imposter distributions indicates false acceptance/rejection: some given samples may be matched falsely. Fig. 10 shows the similarity score distributions of genuine (solid lines) and imposter (dashed lines) fingerprints use two sets of data where the unraveled 3D data yields a better distinction between genuine and imposter scores. Further, let $M(S_m)$ denote the cumulative distribution function (SDF) of the genuine scores and $N(S_n)$ the CDF of the imposter scores. The Detection Error Tradeoff Characteristic (DET) is a plot of the false imposter rate, $FNMR = M(S_m)$, against the false match rate, $FMR = 1 - N(S_n)$, for all values of $S_m$ and $S_n$. The DET, and equivalent Receiver Operating Characteristic (ROC),[33,34] are the most used statement of the performance of the fingerprint verification system. The ROCs of 2D plain and unraveled 3D fingerprints are shown in Fig. 11.

To illustrate the performance of two systems more specifically, we can choose different operating thresholds. And the False Acceptance Rate (FAR) and True Acceptance Rate (TAR) values are computed at each operating threshold. For a generally specific FAR, usually $0.01$, the TAR for the 3D system is $0.97$, while the 2D system is $0.77$. And for a FAR of $0.1$, the TAR of the 3D system is 0.99, while the 2D system is 0.90. Thus, the 3D fingerprint data set achieves a better matching performance in terms of ROC.

## 6 Conclusion

In this paper, we present a thorough evaluation of non-contact 3D fingerprints after unraveling them into 2D equivalent ones, using the quality and matching algorithms developed by NIST, originally proposed for conventional 2D fingerprints. Experimental results demonstrate that the superior quality and matching performance is achieved by the unraveled 3D fingerprint. During the research, we found that the ridge depth information adds additional features to the albedo features based on quality measures. Having the 3D surface information allows for a consistent flattening with the distortions diffused uniformly across the print. Conventional flat prints distort less uniformly and only provide less features being those only against the rigid surface. Thus, the non-contact 3D print outperforms the traditional contact 2D plain counterpart in terms of the number of high quality features and matching

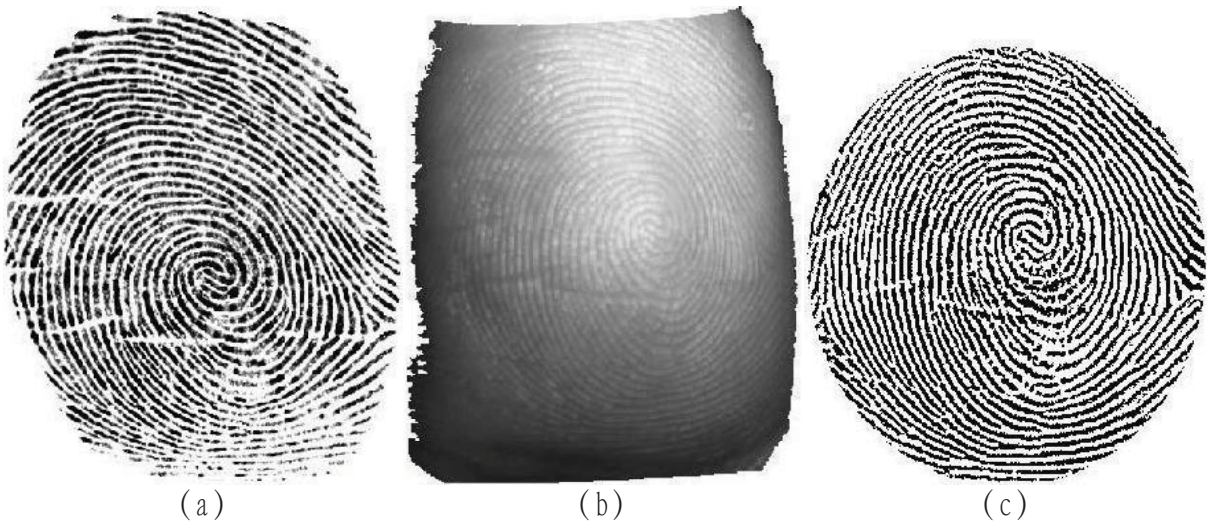


**Fig. 12** The fingerprint scan. (a) A 2D plain fingerprint. (b) The corresponding 3D scan. (c) The 2D unraveled equivalent obtained from 3D scan.

performance.

For visually confirmation of these results, a typical 2D plain fingerprint obtained from the Cogent CSD450 scanner and a typical 3D print are shown in Fig. 12 where, from visual inspection, it can be seen that: 1) for most parts, ridges are clear in both 2D plain and unraveled 3D fingerprints; 2) the 2D plain fingerprint has a small empty area in the top-right part due to a dented scar on the finger; 3) ridges in the unraveled 3D fingerprint are more equally spaced which indicates less distortion in 3D data; and 4) there are several concave scars in the fingerprint where 3D uncovers more ridge information than 2D plain.

Currently, we did not use the gray level 3D because both peak and valley information is present whereas prints on class exclude regions of none contact. Thus, the comparison between 3D flattened gray level prints and conventional prints may be complicated. Future studies will involve gray level print matching. Future research will also extend the present studies with different matching algorithms and future scanner improvements.

Because most 2D print systems operate under the assumption that the print to be compared are obtained using the same sensor and, hence, are restricted in their ability to match or compare print originating from different sensors, the interoperability for 2D sensors has been studied by A. Ross and A. Jain.[35] However, there is little effort has been made for the interoperability between 3D and 2D sensors. And since current fingerprints are traditional 2D ones, the issue of 3D to 2D matching becomes especially important. Thus, we will continue to work on interoperability between 3D and 2D fingerprints.

## *Acknowledgments*

This work is partially funded by Flashscan3D, LLC, Richardson, TX and National Institute of Hometown Security, Somerset, KY.

## *References*

1. Jain, A. K., Ross, A., and Pankanti, S., "Biometrics: A tool for information security," *Trans. Inf. Forensics Security* **1**, 125–143 (Jun 2006).
2. Kumar, B. V. K. V., Savvides, M., Xie, C., Venkataramani, K., Thomton, J., and Mahalanobis, A., "Biometric verification with correlation filters," *Applied Optics* **43**, 391–402 (Jan. 2004).
3. Cappelli, R., Maio, D., Maltoni, D., Wayman, J. L., and Jain, A. K., "Performance evaluation of fingerprint verification systems," *IEEE Transactions on Pattern Analysis and Machine Intelligence* **28**, 3–18 (Jan. 2006).
4. Wu, J. C. and Wilson, C. L., "Nonparametric analysis of fingerprint data on large data sets," *Pattern Recognition* **40**, 2574–2584 (2007).
5. Venkataramani, K. and Kumar, B. V. K. V., "Performance of composite correlation filters in fingerprint verification," *Optical Engineering* **43**, 1820–1827 (Aug. 2004).
6. Fatehpuria, A., Lau, D. L., and Hassebrook, L. G., "Acquiring a 2-d rolled equivalent fingerprint image from a non-contact 3-d finger scan," *Biometric Technology for Human Identification III, SPIE Defense and Security Symposium, Orlando, Florida* **6202**, 62020C–1 – 62020C–8 (Apr. 2006).
7. Hashido, R., Suzuki, A., Iwata, A., Okmoto, T., Satoh, Y., and Inoue, M., "A capacitive fingerprint sensor chip using low-temperature poly-si TFTs on a glass substrate and a novel and unique sensing method," *IEEE J. Solid-State Circuits* **38**, 274–280 (Feb 2003).
8. Sato, N., "Novel surface structure and its fabrication process for MEMS fingerprint sensor," *IEEE Trans. Electron Devices* **52**, 1026–1032 (May 2005).
9. Charlot, B., Parrain, F., Galy, N., Basrour, S., and Courtois, B., "A sweeping mode integrated fingerprint sensor with 256 tactile microbeams," *IEEE J. Microelectromech. Syst.* **13**, 636–644 (Aug 2004).
10. Faundez-Zanuy, M., "Are inkless fingerprint sensors suitable for mobile use," *IEEE Aerosp. Electron. Syst. Mag* **19**, 17–21 (Apr. 2004).
11. Ratha, N. and Bolle, R., "Automatic fingerprint recognition systems," *Sprinter-Verlag* (2004).
12. Ross, A., Dass, S. C., and Jain, A. K., "Estimating fingerprint deformation," *Proceedings of the International Conference on Biometric Authentication (ICBA)* , 249–255 (2004).
13. Roberge, D., Soutar, C., and Kumar, B. V. K. V., "Optimal trade-off filter for the correlation of fingerprints," *Optical Engineering* **38**, 108–113 (Jan. 1999).
14. Chen, X., Tian, J., Yang, X., and Zhang, Y., "An algorithm for distorted fingerprint matching based on local triangle feature set," *IEEE Trans. Inf. Forensics Security* **1**, 169–177 (June 2006).
15. Rowe, R., Corcoran, S., Nixon, K., and Ostrom, R., "Multi-spectral imaging for biometrics," *Proc. SPIE Conf. Spectral Imaging: Instrumentation, Application, and Analysis* , 90–99 (Mar 2005).
16. "Mitsubishi touchless fingerprint sensor,"

*http://global.mitsubishielectric.com* (Oct 2006).
17. Parziale, G., Diaz-Santana, E., and Hauke, R., "The surround imager: A multi-camera touchless device to acquire 3d rolled-equivalent fingerprints," *On Proc. of IAPR Int. Conf. on Biometrics, LNCS* **3832**, 244–250 (Jan 2006).
18. Wang, Y., Lau, D. L., and Hassebrook, L. G., "Fit-sphere unwrapping and performance analysis of 3d fingerprints," *Applied Optics* **49**, 592–600 (Feb. 2010).
19. Chen, Y., Parziale, G., Diaz-Santana, E., and Jain, A. K., "3d touchless fingerprints: Compatibility with legacy rolled images," *Biometric Consortium Conference, 2006 Biometrics Symposium* , 1–6 (2006).
20. Srinivasan, V., Liu, H., and Halioua, M., "Automated phase-measuring profilometry of 3d diffuse objects," *Applied Optics* **23**(18), 3105–3108 (1984).
21. Liu, K., Wang, Y., Lau, D. L., Hao, Q., and Hassebrook, L. G., "Gamma model and its analysis for phase measuring profilometry," *Journal of the Optical Society of America A* **27**, 553–562 (Mar. 2010).
22. Yalla, V. and Hassebrook, L. G., "Very-high resolution 3d surface scanning using multi-frequency phase measuring profilometry," *Spaceborne sensors II, SPIE's defense and security symposium 2005* **5798-09**, 1234–1240 (2005).
23. Salvi, J., Pages, J., and Batlle, J., "Pattern codification strategies in structured light system," *Pattern Recognit.* **37**, 827–849 (Apr. 2004).
24. Li, J., Hassebrook, L. G., and Guan, C., "Optimized two-frequency phase measuring profilometry light-sensor temporal-noise sensitivity," *J. Opt. Soc. Am. A* **20**, 106–115 (Jan 2003).
25. Wang, Y., Liu, K., Lau, D. L., and Hassebrook, L. G., "Multicamera phase measuring profilometry for accurate depth measurement," *SPIE, Orlando, Florida* (Apr 2007).
26. Liu, K., Wang, Y., Lau, D. L., Hao, Q., and Hassebrook, L. G., "Dual-frequency pattern scheme fro high-speed 3-d shape measurement," *Optics Express* **8**, 5229–5244 (Mar. 2010).
27. Tabassi, E., Wilson, C. L., and Watson, C. I., "Fingerprint image quality," *NIST* (Aug 2004).
28. Wu, J. C. and D., G. M., "Nonparametric statistical data analysis of fingerprint minutiae exchange with two-finger fusion," *NISTIR 7376, NIST* (Dec 2006).
29. Almansa, A. and Linderberg, T., "Fingerprint enhancement by shape adaption of scale-space operators with automatic scale selection,"
30. Hong, L., Wan, Y., and Jain, A. K., "Fingerprint image enhancement algorithm and performance evaluation," *IEEE Transactions on Pattern Analysis and Machine Intelligence* **20**, 777–789 (Aug. 1998).
31. Fatehpuria, A., Lau, D. L., Yalla, V., and Hassebrook, L. G., "Performance analysis of three-dimensional ridge acquisition from live finger and palm surface scans," *Proc. SPIE 6539, 653904* (2007).
32. Fatehpuria, A., "Performance evaluation of non-contact 3-d fingerprint scanner," *Master Thesis, University of Kentucky* (Dec 2006).
33. Wu, J. C. and Wilson, C. L., "An empirical study of sample size in roc-curve analysis of fingerprint data," *Proc. of SPIE Vol. 6202, Biometric Technology for Human Identification III, Edited by P.J.Flynn, S.Pankanti* (Apr 2006).
34. Choi, H., Kang, R., Choi, K., Jin, A. T. B., and Kim, J., "Fake-fingerprint detection using multiple static features," *Optical Engineering* **48**, 047202–1–047202–13 (Apr. 2009).
35. Ross, A. and Nadgir, R., "A calibration model for fingerprint sensor interoperability," *Proc. of SPIE Conference on Biometric Technology for Human Identification III (Orlando, USA)* , 62020B–1–62020B–12 (Apr 2006).

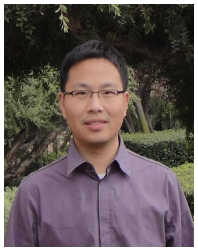

**Yongchang Wang** received his B.E. degree in electrical engineering from Zhejiang University, Hangzhou, China, and his M.S. degree in electrical and computer engineering from University of Kentucky, USA, respectively in 2005 and 2008. Currently, he is working toward his Ph.D. degree in electrical and computer engineering at University of Kentucky. His research interests include biometrics, signal and image processing, and machine and computer vision.

**Qi Hao** received the B.E. and M.E. degrees from Shanghai Jiao Tong University, Shanghai, China, in 1994 and 1997, respectively, both in electrical engineering, and the Ph.D. degree in electrical and computer engineering from Duke University, Durham, NC, in 2006. His postdoctoral training in the Center for Visualization and Virtual Environment, the University of Kentucky, was focused on 3-D computer vision for human tracking and identification. He is currently an Assistant Professor in the Department of Electrical and Computer Engineering, the University of Alabama, Tuscaloosa. His research interests include compressive wireless sensors, intelligent wireless sensor networks, and image processing.

**Abhishika Fatehpuria** received the bachelor's degree in electronics engineering from SRKN college of engineering, Nagpur, India in 2002. She received the MS degree in electrical engineering from University of Kentucky in 2006. She is currently pursuing a PhD degree in electrical engineering from University of Kentucky under the guidance of Dr. Daniel L. Lau. Her research interests include biometrics, fingerprint analysis and image processing.

**Laurence G. Hassebrook** is Blazie Professor of Electrical and Computer Engineering, a Professional Engineer and an active member of the Center for Visualization and Virtual Environments at University of Kentucky. While studying at the Center of Excellence in Optical Processing, he received his Ph.D. degree from Carnegie Mellon University in 1990, his M.S.E.E. from Syracuse University in 1987 and his B.S.E.E. from University of Nebraska in Lincoln, in 1979. He worked at IBM Endicott, New York between 1981 through 1987. His research interests are in 3-Dimensional Data Acquisition, pattern recognition and N-Dimensional signal processing. Current work includes 3-D surface scanning of objects in motion, dynamic pattern projection for multi-target tracking, automatic target recognition, and scene reconstruction from partial images. Dr. Hassebrook has published more than 124 technical papers.

**Daniel L. Lau** received his B.Sc. degree (with highest distinction) in Electrical Engineering from Purdue University, West Lafayette, IN, in 1995 and the Ph.D. degree from the University of Delaware, Newark, in 1999. Today, he is an Associate Professor at the University of Kentucky, Lexington. Prior, he was a DSP Engineer at Aware, Inc., and an Image and Signal Processing Engineer at Lawrence Livermore National Laboratory. His research interests include 3-D imaging sensors, 3-D fingerprint identification, and multispectral color acquisition and display. His published works in halftoning include the introduction of the green-noise halftoning model as well as stochastic moire. Aside from his research interests, Dr. Lau is also an avid artist specializing in lenticular photography.